Hierarchical Self-Assembly of Poly(γ-benzyl-L-glutamate)−Poly(ethylene glycol)−Poly(γ-benzyl-L-glutamate) Rod−Coil−Rod Triblock Copolymers

G. Floudas*,† and P. Papadopoulos

Department of Physics, University of Ioannina, and Foundation for Research and Technology-Hellas, Biomedical Research Institute (FORTH−BRI), P.O. Box 1186, 451 10 Ioannina, Greece

H.-A. Klok,*,‡,§ G. W. M. Vandermeulen, and J. Rodriguez-Hernandez

Max Planck Institut für Polymerforschung, D-55021 Mainz, Germany

Received December 5, 2002; Revised Manuscript Received March 11, 2003

ABSTRACT: The self-assembly mechanism has been studied in poly(γ-benzyl-L-glutamate)−poly(ethylene glycol)−poly(γ-benzyl-L-glutamate) (PBLG−PEG−PBLG) triblock copolymer melts using X-ray scattering, polarizing optical microscopy, differential scanning calorimetry, and FTIR spectroscopy. Intrinsic competing interactions (crystallization, hydrogen bonding, liquid crystallinity, microphase separation) give rise to different levels of organization. Depending on the peptide volume fraction *f*, two cases can be discussed: for low peptide volume fractions, microphase separation results in PBLG and PEG phases rich in all secondary structures (α-helices, β-sheets, and chain-folded PEG) notwithstanding the large undercooling necessary to induce PEG crystallization. For $f > 0.4$, interfacial mixing results in the destruction of the less coherent peptide secondary structures (β-sheet). Interfacial mixing may prove to be a key factor in controlling the appearance of β-sheets in low molecular weight peptides.

1. Introduction

Self-assembly is the key in the design of new functional materials. Macromolecules with well-defined structures on the nanometer scale are perfect candidates for self-assembled materials and nanometer scale devices. Of key importance for the control of self-organization in such systems is the combination of antagonistic interactions that can result in materials possessing order over multiple length scales.[1,2]

The present study combines the elegant complexity of biological macromolecules with the relatively simpler nature of synthetic polymers aiming to design new functional materials with controlled internal dimensions and structures ranging from nanometer to macroscopic scales. For this purpose we employ the basic ingredients favoring self-assembly: (1) crystallization, (2) hydrogen bonding, (3) liquid crystallinity, and (4) microphase separation. The system consists of the synthetic water-soluble semicrystalline polymer poly(ethylene glycol) (PEG), i.e., one of the most well-studied homopolymers that self-assemble by chain folding.[3] PEG upon crystallization orders over different length scales; from the monoclinic unit cell with a helical chain conformation (∼1 nm) to lamellar stacks separated by amorphous chains (∼10 nm) and to the macroscopic superstructures known as spherulites (up to several micrometers). The second macromolecule is of biological origin and is based on the well-known polypeptide poly(γ-benzyl-L-glutamate) (PBLG), where inter- and intramolecular hydrogen bonds stabilize the secondary structures. PBLG is a typical helical polypeptide with a stiff rigid-rod structure which shows mesoscopic liquid crystal order.[4] Because of its good solubility and rodlike structure, it has been extensively studied with respect to its helix-to-coil transition and liquid crystalline properties.[5−7] It shows two secondary structures (α-helices and β-sheets) with populations depending on the polypeptide length. In particular, aggregated β-sheet structures have been associated with amyloid and prion diseases.[8] Thus, the development of controlled conditions and of structures favoring their presence or absence may prove to be important in biomedical and biophysical applications.

In the present system, the two inherently organized homopolymers form the building blocks of a triblock copolymer composed of PBLG−PEG−PBLG. It is of interest to explore how the intrinsic tandem molecular interactions present within and between the blocks (crystallization, peptide secondary structure, microphase separation) can stabilize certain structures and give rise to new materials with specific structures and functions. The synthesis of PBLG−PEG−PBLG triblock copolymers has been reported before.[9−11] Studies on the nanoscale solid-state organization in such triblock copolymers are, however, scarce and essentially limited to thin films covering a small number of compositions.[11] In the present study, we present a detailed structural investigation of the hierarchical self-assembly in 13 PBLG−PEG−PBLG triblock copolymers. We found that the incorporation of a water-soluble synthetic polymer next to the peptide block provides a way of controlling the stability of a specific peptide secondary structure.

2. Experimental Section

Materials. *N*,*N*′-Dimethylformamide (DMF) was distilled from CaH_2 under reduced pressure and subsequently stored over molecular sieves (4 Å) under an argon atmosphere. Poly(ethylene glycol) (PEG) was dried by azeotropic distillation in toluene (three times). γ-Benzyl-L-glutamate *N*-carboxyanhydride (Bn-Glu NCA) (compound **4** in Scheme 1, below) was prepared according to a literature procedure.[12] The synthesis of the poly(γ-benzyl-L-glutamates) (PBLG) homopolymers **18**−**26** has been described elsewhere.[13,14] All other chemicals were purchased from Sigma Aldrich Chemie GmbH (Deisenhofen, Germany) and used as received.

† E-mail: gfloudas@cc.uoi.gr.
‡ E-mail: hak@mpip-mainz.mpg.de.
§ Present address: Laboratoire des Polymères, Institut des Matériaux, Ecole Polytechnique Fédéral de Lausanne. CH-1015 Lausanne, Switzerland. E-mail: harm-anton.klok@epfl.ch.

10.1021/ma025918k CCC: $25.00
Published on Web 04/18/2003

Scheme 1

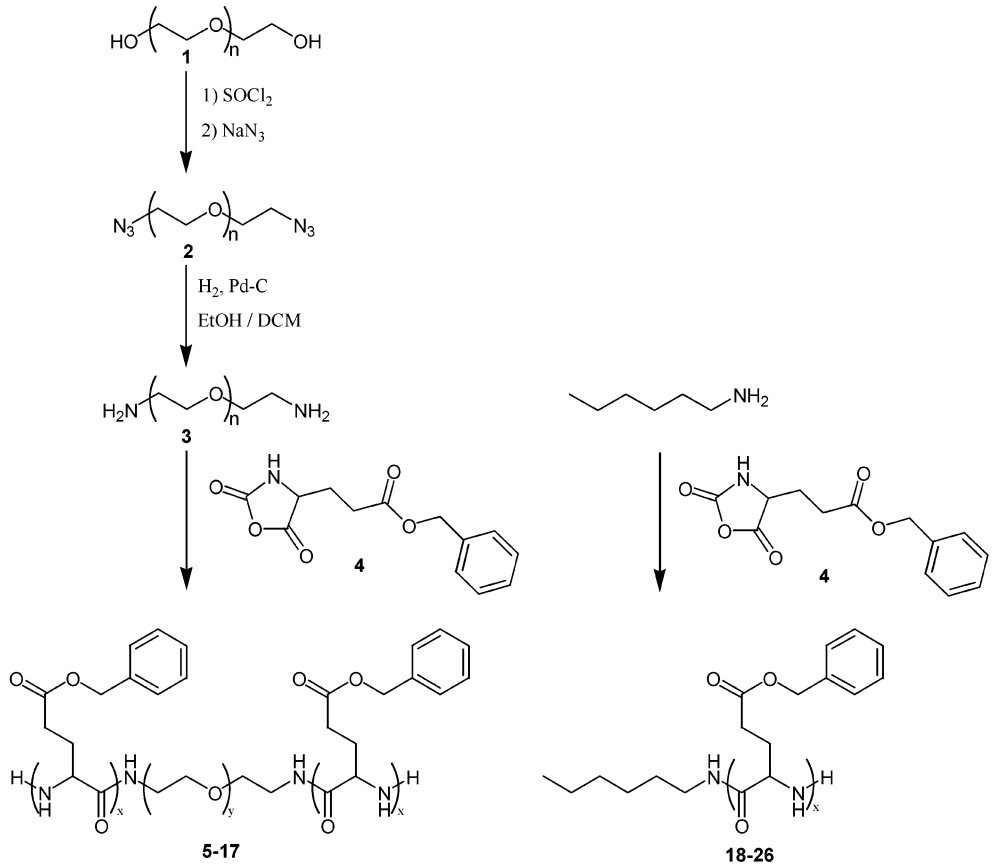

Procedures. Poly(ethylene glycol) Dichloride (PEG-Cl_2) (1). Poly(ethylene glycol) was dissolved in 40 molar equiv of thionyl chloride under argon atmosphere. The suspension was refluxed for 12 h at 363 K. Then, the mixture was allowed to cool to room temperature and evaporated until dryness. The residue was dissolved in a small amount of dichloromethane and precipitated with a large excess of cold diethyl ether. Filtration and drying under reduced pressure gave the desired poly(ethylene glycol) dichloride.

PEG1000-Cl_2 (**1a**). Yield: 95%. ^{1}H NMR ($CDCl_3$): $\delta = 3.73$ ppm (4H, t, $-CH_2CH_2Cl$), 3.71 ppm (4H, t, $-CH_2CH_2Cl$), 3.60 ppm (84H, $-CH_2CH_2O$).

PEG4000-Cl_2 (**1b**). Yield: 94%. ^{1}H NMR ($CDCl_3$): $\delta = 3.73$ ppm (4H, t, $-CH_2CH_2Cl$), 3.71 ppm (4H, t, $-CH_2CH_2Cl$), 3.60 ppm (360H, $-CH_2CH_2O$).

PEG6000-Cl_2 (**1c**). Yield: 96%. ^{1}H NMR ($CDCl_3$): $\delta = 3.73$ ppm (4H, t, $-CH_2CH_2Cl$), 3.71 ppm (4H, t, $-CH_2CH_2Cl$), 3.60 ppm (552H, $-CH_2CH_2O$).

Poly(ethylene glycol) Diazide (PEG-$(N_3)_2$) (2). Poly(ethylene glycol) dichloride (**1**) was dissolved at 333 K in DMF. To this solution was added a 10-fold excess of NaN_3, and the resulting mixture was refluxed for 4 h at 413 K. After evaporation of the solvent, the residue was dissolved in dichloromethane and washed twice with water. The aqueous phase was extracted three times with dichloromethane and the combined organic phases were dried with $MgSO_4$. The dried solution was filtered and the solvent evaporated. The product was precipitated from dichloromethane with cold diethyl ether to give poly(ethylene glycol) diazide in a yield of 66−92%.

PEG1000-$(N_3)_2$ (**2a**). Yield: 66%. ^{1}H NMR ($CDCl_3$): $\delta = 3.60$ ppm (84H, $-CH_2CH_2O$), 3.35 ppm (4H, t, $-CH_2N_3$).

PEG4000-$(N_3)_2$ (**2b**). Yield: 92%. ^{1}H NMR ($CDCl_3$): $\delta = 3.60$ ppm (360H, $-CH_2CH_2O$), 3.35 ppm (4H, t, $-CH_2N_3$).

PEG6000-$(N_3)_2$ (**2c**). Yield: 83%. ^{1}H NMR ($CDCl_3$): $\delta = 3.60$ ppm (552H, $-CH_2CH_2O$), 3.35 ppm (4H, t, $-CH_2N_3$).

Poly(ethylene glycol) Diamine (PEG-$(NH_2)_2$) (3). Poly(ethylene glycol) diazide (**2**) was dissolved in a small amount of an ethanol−dichloromethane (4/1) mixture. After addition of an equal amount of 10% Pd−C, the mixture was stirred under H_2 atmosphere for 18 h. Afterward, the mixture was filtered over Hyflo to remove the catalyst. Evaporation of the solvents and subsequent precipitation with cold diethyl ether afforded poly(ethylene glycol) diamine in 80−90% yield. When MALDI−TOF mass spectrometry still showed the presence of poly(ethylene glycol) monoamine or poly(ethylene glycol) diazide, the above procedure was repeated until completion.

PEG1000-$(NH_2)_2$) (**3a**). Yield: 80%. ^{1}H NMR ($CDCl_3$): $\delta = 3.60$ ppm (84H, $-CH_2CH_2O$), 3.10 ppm (4H, t, $-CH_2NH_2$). MALDI−TOF MS: $M_w = 1234$ g/mol, $M_n = 1164$ g/mol, and $M_w/M_n = 1.06$.

PEG4000-$(NH_2)_2$) (**3b**). Yield: 90%. ^{1}H NMR ($CDCl_3$): $\delta = 3.60$ ppm (360H, $-CH_2CH_2O$), 2.90 ppm (4H, t, $-CH_2NH_2$). MALDI−TOF MS: $M_w = 4005$ g/mol, $M_n = 3960$ g/mol, and $M_w/M_n = 1.01$.

PEG6000-$(NH_2)_2$) (**3c**). Yield: 91%. ^{1}H NMR ($CDCl_3$): $\delta = 3.60$ ppm (552H, $-CH_2CH_2O$), 2.90 ppm (4H, t, $-CH_2NH_2$). MALDI−TOF MS: $M_w = 5692$ g/mol, $M_n = 5747$ g/mol, $M_w/M_n = 1.01$.

PBLG—PEG—PBLG Triblock Copolymers (5—17). γ-Benzyl-L-glutamate *N*-carboxyanhydride was dissolved in dry DMF (~0.3 g/mL) under argon atmosphere. Then, a solution of PEG-$(NH_2)_2$ (**3**) in dry DMF (0.1 g/mL) was added, and the resulting solution was stirred for 5 d at room temperature. The solvent was evaporated, the residue was taken up in dichloromethane, and precipitation with cold diethyl ether resulted in the triblock copolymer as a white solid. Yields were 80−90%. As a representative example, the results of the NMR characterization of **5** are given below:

^{1}H NMR ($CDCl_3$): $\delta = 7.35-7.10$ ppm (50H, H_{arom}), 5.12−4.88 ppm (20H, s, H_{benzyl}), 4.02−3.79 ppm (10H, m, H_α-Glu), 3.68−3.51 ppm (80H, CH_2CH_2O), 2.70−2.46 ppm (20H, m, H_γ-Glu), 2.45−2.14 ppm (20H, m, H_β-Glu).

Methods. Gel Permeation Chromatography (GPC). GPC was performed at 333 K with a setup consisting of a Waters 510 pump and a series of three styrene-divinylbenzene

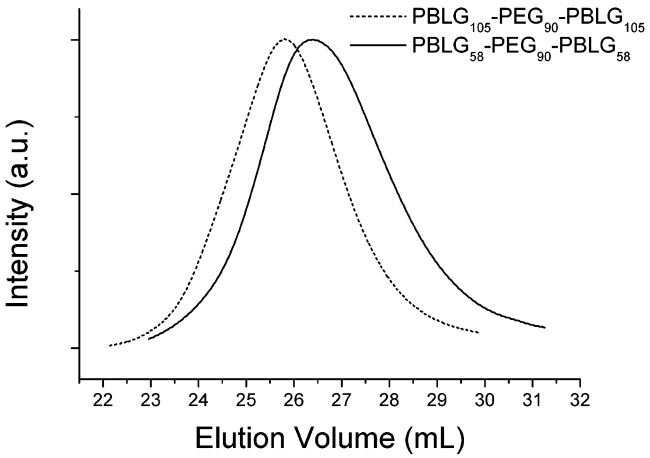

Figure 1. GPC traces (refractive index detector signal) of $PBLG_{58}$−PEG_{90}−$PBLG_{58}$ and $PBLG_{105}$−PEG_{90}−$PBLG_{105}$ triblock copolymers.

(SDV) columns (300 × 8 mm) with pore sizes of 500, 10^5, and 10^6 Å (Polymer Standards Service). A 0.1 M solution of LiBr in DMF was used as the mobile phase and the elution of the samples was monitored with refractive index (RI) detection. Elution times were converted to molecular weights with a calibration curve constructed from narrow polydispersity polystyrene standards.

NMR Spectroscopy. NMR spectra were recorded at room temperature on a Bruker Advance 250 spectrometer using the residual proton resonance of the deuterated solvent as the internal standard.

MALDI—TOF Mass Spectroscopy. MALDI−TOF mass spectra were acquired on a Bruker Reflex II MALDI−TOF spectrometer. Samples were dissolved in tetrahydrofuran (THF) and mixed with the matrix dithranol. Sodiumtrifluoroacetate was added to generate positive ions.

Fourier Transform Infrared (FTIR) Spectroscopy. Transmission-FTIR spectra were measured with a Nicolet Magna IR 850 spectrometer, using a triglycine−sulfate (TGS) detector (resolution, 4 cm^{-1}; number of scans, 128) equipped with a temperature control unit. The sample and detector chamber were purged with dry air before and during the measurement. IR films were prepared by dissolving a 20% (w/v) solution of triblock copolymer or PBLG homopolymer in DMF and subsequent spin-coating on a silicon wafer. Only films with a transmission below 10% were used. Films were heated at 433 K and allowed to equilibrate for 1 h before measurement. This procedure was repeated for all chosen temperatures, i.e., 393, 373, 333, 313, and 303 K. The temperature levels were maintained with an accuracy of ±0.5 K.

Polarizing Optical Microscopy. A Zeiss Axioskop 2 polarizing optical microscope was used together with a Linkam heating stage (THMS 600) and a TP93 temperature programmer (heating and cooling rates of 0.1−90 K/min). The system is also capable of monitoring the kinetics in real time by continuous recording using a CCD camera ($^1/_2$ in. Sony color camera) and a fast frame grabber (capable of up to 50 frames/s) which allows an analysis in terms of the nucleation density, shape and growth rates using with an appropriate software (Image Pro Plus). The experiments were made by heating to an initial temperature (T_i = 433 K) corresponding to the melt state of semicrystalline PEG, followed by subsequent cooling to temperatures corresponding to the crystalline (PEG) or liquid crystalline structures (PBLG). Subsequently, images were taken while heating. Representative images for PEG_{90}, $PBLG_{18}$ and the copolymer $PBLG_{17}$−PEG_{90}−$PBLG_{17}$ are shown in Figure 2 at 303 K. The PEG image exhibits the usual spherulitic structure with a low nucleation density. The peptide pattern, on the other hand, shows some singular points, i.e., disclinations that are due to discontinuities in orientation of phases. Such points are normally observed in nematic liquid crystals. We should mention here that in

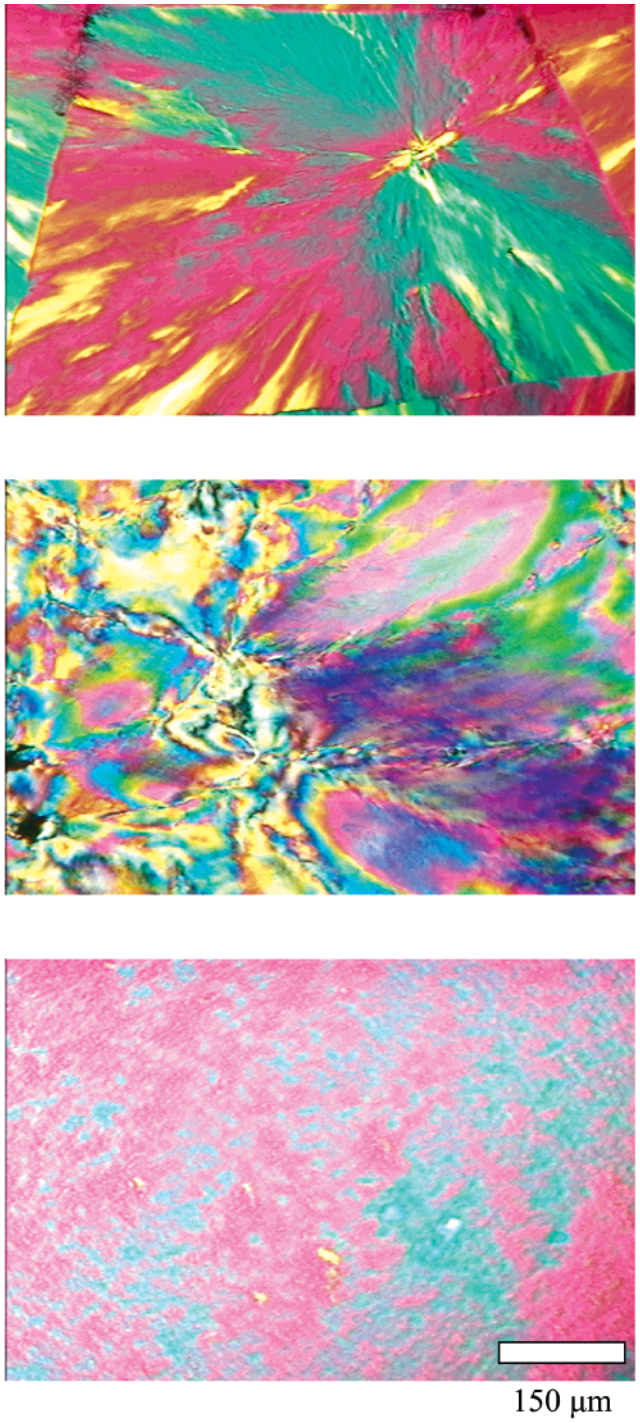

Figure 2. Polarizing optical microscopy images, taken at 303 K: PEG_{90} (top), $PBLG_{18}$ (middle), and $PBLG_{17}$−PEG_{90}−$PBLG_{17}$ triblock copolymer (bottom). Notice that the usual spherulitic superstructure in the PEG homopolymer is absent in the copolymer that exhibits a weak liquid crystalline order.

monodisperse polypeptides a smectic mesophase has also been observed. On the other hand, the copolymer shows only a weak liquid crystalline order in the absence of any spherulitic superstructure. Apparently, the PEG midblock did not crystallize in the triblock under conditions of undercooling (ΔT = 40 K) that would favor the homopolymer crystallization. This issue will be explored in detail below.

Differential Scanning Calorimetry. A Mettler Toledo Star DSC capable of programmed cyclic temperature runs over the range 113−673 K was used. Samples were first heated with a rate 10 K/min to temperatures corresponding to the melt state and subsequently cooled to 153 K with the same

Table 1. Molecular Characteristics of the PBLG−PEG−PBLG Triblock Copolymers and Peptides Investigated in This Study

compound no.	compound name	M_n PEG block[a] (g/mol)	$N_{n,PEG}$[a]	M_n PBLG block[b] (g/mol)	$N_{n,PBLG}$ block[b]	f_{PBLG}[c]
5	$PBLG_5-PEG_{21}-PBLG_5$	940	21	1095	5	0.295
6	$PBLG_9-PEG_{21}-PBLG_9$	940	21	1970	9	0.43
7	$PBLG_{22}-PEG_{21}-PBLG_{22}$	940	21	4820	22	0.65
8	$PBLG_{54}-PEG_{21}-PBLG_{54}$	940	21	11 830	54	0.82
9	$PBLG_{96}-PEG_{21}-PBLG_{96}$	940	21	21 020	96	0.89
10	$PBLG_4-PEG_{90}-PBLG_4$	3980	90	880	4	0.07
11	$PBLG_8-PEG_{90}-PBLG_8$	3980	90	1750	8	0.135
12	$PBLG_{17}-PEG_{90}-PBLG_{17}$	3980	90	3720	17	0.25
13	$PBLG_{58}-PEG_{90}-PBLG_{58}$	3980	90	12 700	58	0.53
14	$PBLG_{105}-PEG_{90}-PBLG_{105}$	3980	90	23 000	105	0.67
15	$PBLG_4-PEG_{138}-PBLG_4$	6090	138	880	4	0.048
16	$PBLG_9-PEG_{138}-PBLG_9$	6090	138	1970	9	0.1
17	$PBLG_{16}-PEG_{138}-PBLG_{16}$	6090	138	3500	16	0.17
18	$PBLG_7$			1630	7	
19	$PBLG_8$			1864	8	
20	$PBLG_{14}$			3170	14	
21	$PBLG_{18}$			4045	18	
22	$PBLG_{45}$			9967	45	
23	$PBLG_{49}$			10 840	49	
24	$PBLG_{67}$			14 790	67	
25	$PBLG_{109}$			24 000	109	
26	$PBLG_{140}$			30 860	140	

[a] According to ^{1}H NMR. [b] According to ^{1}H NMR. This is the value for one PBLG block. Note that each triblock copolymer contains two PBLG segments. [c] $f_{PBLG} = N_{n,PBLG}^*/(N_{n,PBLG}^* + N_{n,PEG}^*)$; $N_{n,PBLG}^* = N_{n,PBLG}(\rho_{PEG}/\rho_{PBLG})^{1/2}$; $\rho_{PEG} = 1.12$ g/cm^3, $\rho_{PBLG} = 1.278$ g/cm^3 (for α-helical conformations).

rate. The transition temperatures and enthalpies were obtained from the second heating run with the same rate.

X-ray Scattering. Both wide-angle and small-angle X-ray scattering (WAXS and SAXS) measurements have been performed. For the WAXS measurements a Siemens $\theta-\theta$ diffractometer (model D500T) was used in the reflection geometry. The Cu Kα radiation was used from a Siemens generator (Kristalloflex 710 H) operating at 35 kV and 30 mA, and a graphite monochromator was utilized in front of the detector ($\lambda = 0.154$ nm). Measurements were made in the 2θ range from 0.1 to 40° in steps of 0.01°. The following thermal history was employed: first the samples were heated to 433 K and subsequently slowly cooled to 303 K. Diffractograms were taken at 433, 393, 373, 333, 313, and 303 K for all samples. For some cases, the thermal reversibility was checked by slowly heating to 433 K and by acquiring images at the same temperatures. SAXS measurements were performed using an 18 kW rotating anode X-ray source with a pinhole collimation and a two-dimensional detector with 1024 × 1024 pixels. The sample-to-detector distance was 1.46 m. Measurements of 4 h long were made by cooling from 423 to 303 K. In addition, simultaneous SAXS/WAXS measurements were performed at the X27C beamline at the National Synchrotron Light Source at Brookhaven National Laboratory. The wavelength was 0.1366 nm and the sample-to-detector distances were 0.87 and 0.15 m for the SAXS and WAXS measurements, respectively. In WAXS, the position sensitive detector was set at an angle of 45° to the sample. Different experiments have been performed. First the samples were preheated to 453 K, to erase any thermal history effects, and subsequently cooled slowly (with 2 K/min) to 313 K. During the cooling and the subsequent heating runs back to 453 K (with the same rate) SAXS/WAXS images were obtained in 1 min intervals. In a second experiment, the kinetics of phase transformation were studied in the copolymers by performing T-jump experiments between 453 and 313 K. In these experiments a dual cell temperature jump unit, available at the beamline, was used.

3. Results and Discussion

The synthesis of the PBLG−PEG−PBLG triblock copolymers and PBLG homopolypeptides is outlined in Scheme 1. The α,ω-diamino poly(ethylene glycols) (**3**) were prepared according to a slight modification of a procedure previously published by Zalipsky et al.[15] Subsequently, the α,ω-diamino poly(ethylene glycols) and *n*-hexylamine were used as initiators for the ring-opening polymerization of γ-benzyl-L-glutamate *N*-carboxyanhydride (Bn-Glu NCA) (**4**) to afford the desired PBLG−PEG−PBLG triblock copolymers and homopolypeptides, respectively. The PBLG homopolymers and PBLG−PEG−PBLG triblock copolymers were analyzed by ^{1}H NMR spectroscopy and GPC. The molecular characteristics of the triblock copolymers and homopolypeptides are summarized in Table 1. Since the GPC experiments were performed using a refractive index (RI) detector and narrow polydispersity polystyrene samples as calibration standards, they were not expected to provide useful quantitative molecular weight information and the data listed in Table 1 refer to the results from the ^{1}H NMR experiments. The GPC results, however, are useful to verify the absence of homopolymer impurities. As a representative example, GPC traces of $PBLG_{58}-PEG_{90}-PBLG_{58}$ and $PBLG_{105}-PEG_{90}-PBLG_{105}$ are shown in Figure 1. Polydispersities of the PBLG homopolypeptides and the PBLG−PEG−PBLG triblock copolymers, as estimated from GPC, were 1.1−1.5 and 1.3−1.6, respectively. These relative narrow molecular weight distributions are most likely due to fractionation of the samples during precipitation.

Already the results from polarizing optical microscopy revealed substantially different structures on a macroscopic scale (resolution ∼2 μm) in the triblocks as compared to the two homopolymers. The images in Figure 2 revealed that in the $PBLG_{17}-PEG_{90}-PBLG_{17}$ triblock the PEG midblock did not crystallize, despite the large undercooling. This constitutes the first, macroscopic evidence, for the existence of structural changes in the triblocks as opposed to the homopolymers. As we will see below, these macroscopic changes reflect on thermodynamic changes imposed by the tandem molecular interactions on smaller length scales.

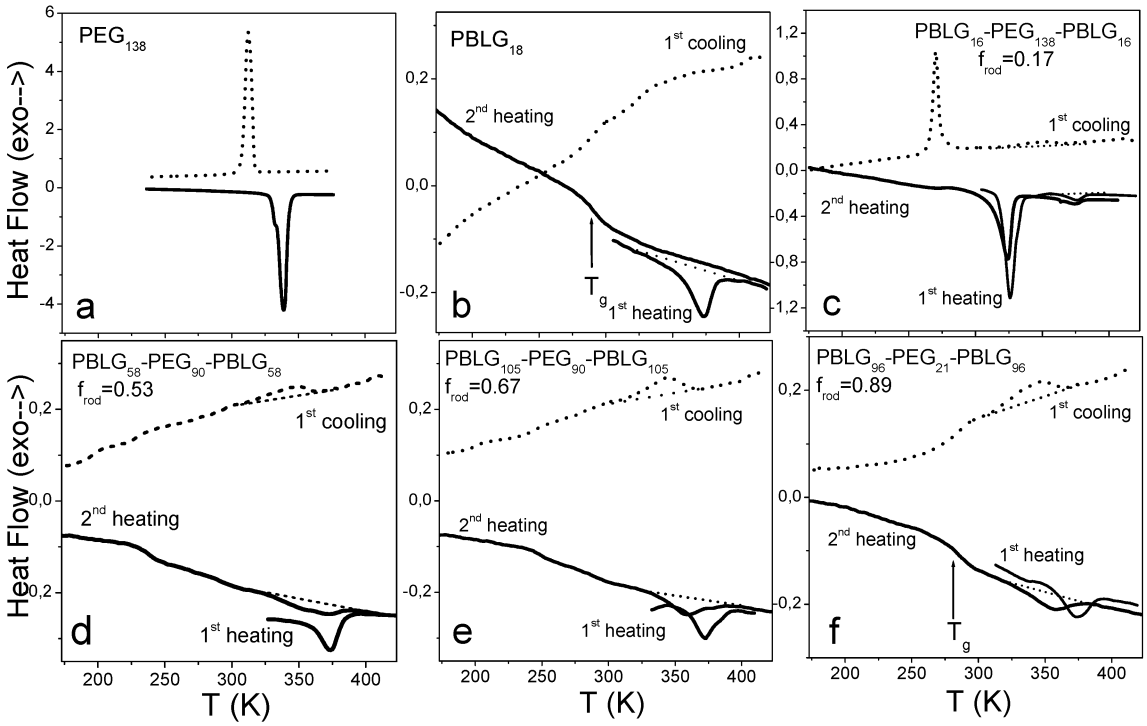

Figure 3. DSC thermograms of (a) the PEG_{138} homopolymer, (b) the $PBLG_{18}$, and four triblock copolymers: (c) $PBLG_{16}$−PEG_{138}−$PBLG_{16}$ (f_{rod} = 0.17), (d) $PBLG_{58}$−PEG_{90}−$PBLG_{58}$ (f_{rod} = 0.53), (e) $PBLG_{105}$−PEG_{90}−$PBLG_{105}$ (f_{rod} = 0.67), and (f) $PBLG_{96}$−PEG_{21}−$PBLG_{96}$ (f_{rod} = 0.89). Solid and dashed lines indicate heating and cooling runs, respectively. For the $PBLG_{18}$ and the copolymers, both the first and second heating runs are shown. Notice the first-order transition during the first heating of the pure peptide that is absent in the second heating run. In addition, notice the large undercooling necessary for the PEG crystallization in the $PBLG_{16}$−PEG_{138}−$PBLG_{16}$ (c) and notice that this feature (i.e., the PEG crystallization) is completely absent in the copolymers with the higher peptide content (d−f).

The DSC results, shown in Figure 3, are more enlightening with respect to the imposed thermodynamic changes. The PEG homopolymer crystallization and melting curves obtained with the same rate (10 K/min) reveal a crystallization and apparent melting temperatures at 316 and 336 K, respectively, i.e., an undercooling of 20 K. From the heat of fusion (ΔH = 177 J/g) a degree of crystallinity of about 85% is obtained (ΔH_∞ = 205 J/g).[16] For the pure peptide ($PBLG_{18}$) there is considerable difference between the first heating run and the second heating run. In the first heating run the endothermic peak with a heat of fusion of 10 J/g reflects the first-order transformation between two helical conformations: from a 7/2 to an 18/5 α-helical conformation.[13,17] The α-helix, stabilized by intramolecular hydrogen bonds, has its residues on a spiral pitch of approximately 0.54 nm, which is right-handed for L-α-amino acids and has about 3.6 residues per turn, giving 18 residues in five turns. This α-helical secondary conformation is the norm for peptides. However, a second helical conformation has been reported with seven residues in two turns (7/2). The unusual (7/2) helices are transformed to the normal (18/5) helices via a broad first-order transformation at about 373 K. The transformation is irreversible in the peptides (at least within the time scale of the DSC experiments) as seen by the absence of this feature in the second heating run.

In the copolymers, depending on the peptide volume fraction, two cases can be distinguished. When the peptide volume fraction is below 0.26, the PEG can crystallize but under very high undercooling conditions. For example, in $PBLG_{16}$−PEG_{138}−$PBLG_{16}$ with f_{rod} = 0.17, an undercooling of 52 K is necessary to initiate the PEG crystallization. Such high undercooling parameter is the norm for the block crystallization in nanoconfined structures.[18−20] When the peptide volume fraction exceeds about 0.3, the PEG midblock cannot crystallize even under extreme undercooling conditions ($\Delta T\sim$ 250 K). This inability of PEG chain folding is depicted in Figure 3 for three copolymers: $PBLG_{58}$−PEG_{90}−$PBLG_{58}$ (f_{rod} = 0.53), $PBLG_{105}$−PEG_{90}−$PBLG_{105}$ (f_{rod} = 0.67), and $PBLG_{96}$−PEG_{21}−$PBLG_{96}$ (f_{rod} = 0.89). Notice that in the copolymer heating/cooling traces there is a weak endothermic peak at about 355 K with a heat of fusion in the range 2−5 J/g. This feature reflects that the irreversible 7/2 to 18/5 helical transformation in PBLG becomes reversible in the copolymers. In addition, there exists a glass transition for the pure peptide at 294 K with an associated change in specific heat of Δc_p = 0.42 J/(g K). This transition was found to depend on the peptide length, and the detailed investigation of the peptide dynamics using dielectric spectroscopy will be the subject of a future study.[21] This transition in the copolymers with the higher peptide content was found to shift to lower temperatures indicating some local mixing.

The DSC results revealed some unanticipated structural changes in the copolymers when compared to the homopolymers; nevertheless, a direct structural probe is needed. For this purpose, we employed different scattering techniques capable of revealing the organization at the different length scales. Figure 4 gives the WAXS patterns of $PBLG_{18}$ obtained on cooling from 433 to 303 K. The diffraction patterns reveal that the short peptide chains in $PBLG_{18}$ are composed of a mixture of ordered secondary structures together with disordered structures. The sharp diffraction peaks at smaller scattering angles can be classified according to the two major peptide secondary structures: α-helices and

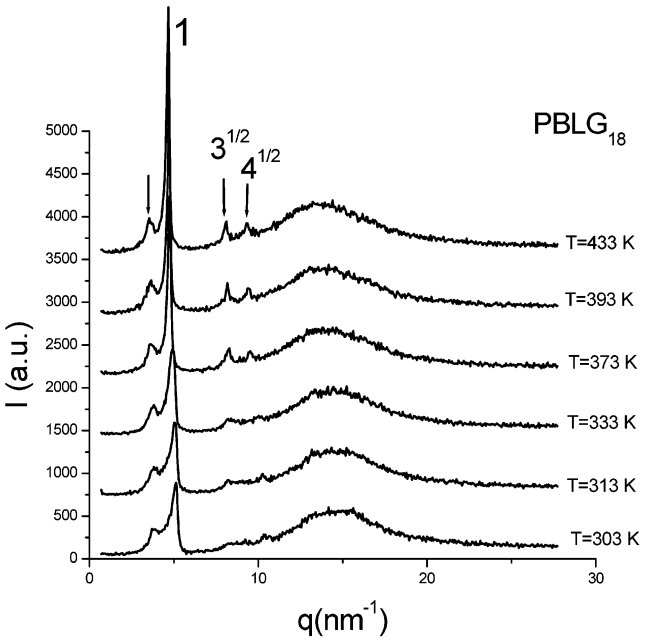

Figure 4. Wide-angle X-ray diffraction patterns of $PBLG_{18}$ shown at different temperatures in the range 433−303 K. The arrows indicate the main reflection and the associated higher order reflections with relative positions $1:3^{1/2}:4^{1/2}$ from a hexagonal arrangement of α-helices. The reflection at $q \sim 3.5$ nm^{-1} associates with the lamellar spacing of β-sheets with an orthogonal unit cell.

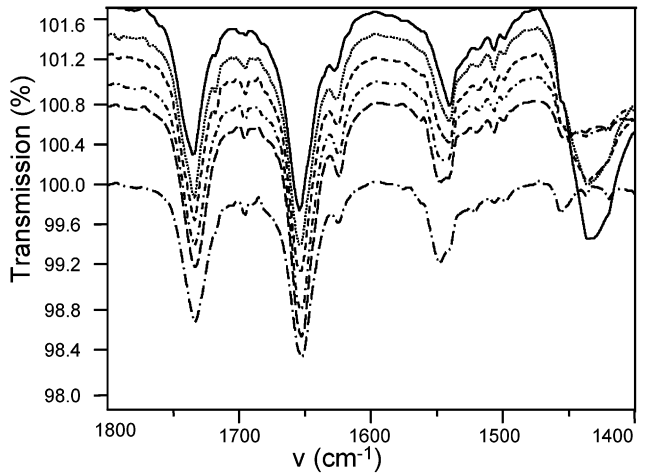

Figure 5. FTIR spectra of the $PBLG_{18}$ homopolymer taken at identical temperatures with the WAXS data and under identical thermal conditions. The amide I and amide II bands at 1655 and 1550 cm^{-1}, respectively, associate with the α-helical conformations whereas the band at 1630 cm^{-1} is the shifted component of the amide I band associated with the β-sheet chain conformations.

β-sheets. The first peak at approximately 3.52 nm^{-1} (distance of 1.78 nm) reflects the distance between backbones in the antiparallel β-pleated sheet structure that is stabilized by intermolecular hydrogen bonds. The assignment is based on the (020) plane of the orthogonal unit cell with the β-conformations.[22] This peak is the predominant secondary structure in the peptides with low (<10) degrees of polymerization. The three remaining reflections (with a $q^* \sim 4.65$ nm^{-1}, distance of 1.35 nm) can be indexed according to a hexagonal packing of cylinders composed of 18/5 α-helices. The pitch of the helix of 0.54 nm is expected to give rise to a weak reflection at 11.6 nm^{-1}. The broad "amorphous halo" centered around 14 nm^{-1} (with a corresponding average

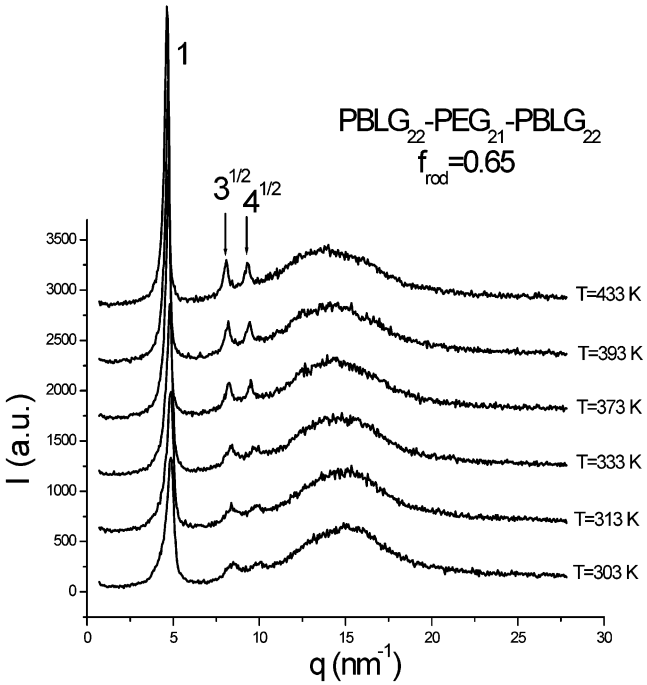

Figure 6. Wide-angle X-ray diffraction patterns of the $PBLG_{22}-PEG_{21}-PBLG_{22}$ triblock copolymer shown at different temperatures in the range 433−303 K. The arrows indicate the main reflection and the associated higher order reflections with relative positions $1:3^{1/2}:4^{1/2}$ from a hexagonal arrangement of α-helices. Notice the absence of the β-sheet secondary structure from the peptide organization in the triblock.

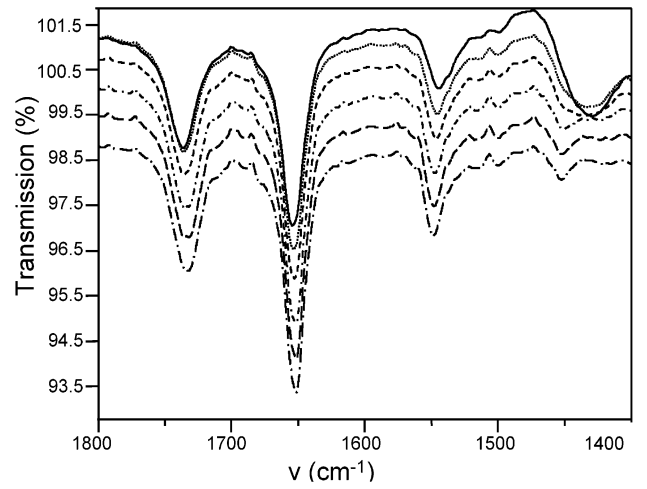

Figure 7. FTIR spectra of the $PBLG_{22}-PEG_{21}-PBLG_{22}$, triblock copolymer, taken at identical temperatures with the WAXS data and under identical thermal conditions. Notice the absence of the amide bands from the spectra related to the β-sheet secondary structure.

distance of 0.45 nm), carries a large fraction of the diffracted intensity originating from the long amorphous side chains. To this end, our solid-state NMR results on a longer PBLG (sample 21 of Table 1) revealed that most of the peptide chains adopt the α-helical conformation. However, there exists both structural and dynamic evidence for randomness within the helices. Two-dimensional WAXS on well-oriented fibers[23] prepared from a chloroform solution, displayed meridional layered lines and reflections on the equator. The absence of Bragg reflections from the layered lines suggests a nematic-like paracrystalline structure composed of a periodic packing of α-helices perpendicular to the chain

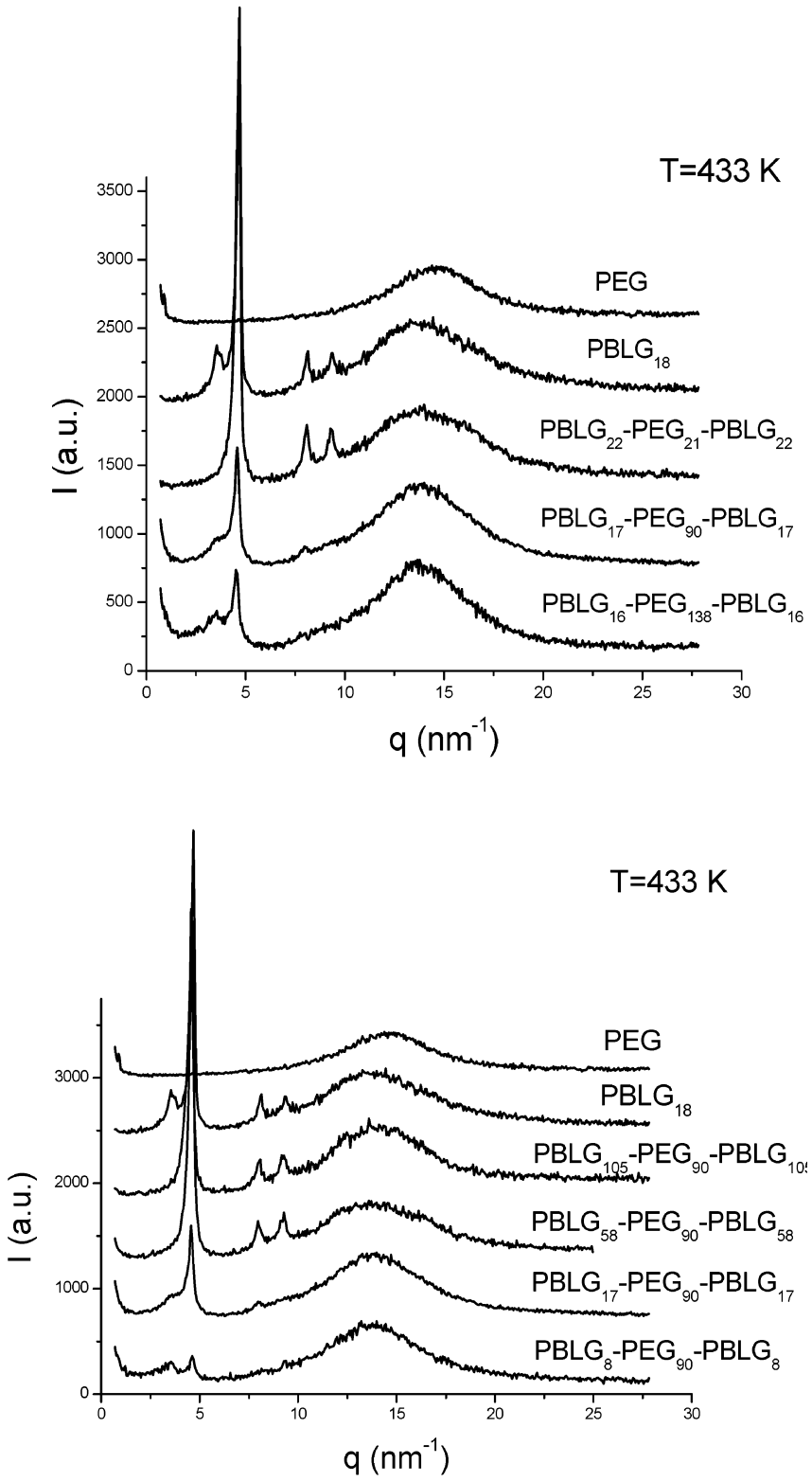

Figure 8. Top: Effect of increasing the PEG degree of polymerization on the WAXS profiles of three copolymers at 433 K. Bottom: Effect of increasing the PBLG degree of polymerization on the WAXS profiles of four copolymers at 433 K. The homopolymer spectra are also shown for comparison.

axis, but with displaced α-helices along the chain axes together with randomness in their orientation. Furthermore, recent dielectric spectroscopy results[21] suggest the existence of a small function of random coil peptides. With respect to Figure 4, notice the strong T dependence of the intensities of the different structures that tend to decrease by lowering temperature as the T_g is approached. The analysis of the spectra will be discussed later (with respect to Figure 9).

The assignment of the peptide secondary structures was confirmed by independent Fourier transform infrared spectroscopy (FTIR) measurements. Figure 5 shows temperature-dependent FTIR spectra of $PBLG_{18}$ following exactly the same thermal history as with the WAXS measurements. The amide I and amide II bands at 1655 and 1550 cm^{-1}, respectively, associate with the

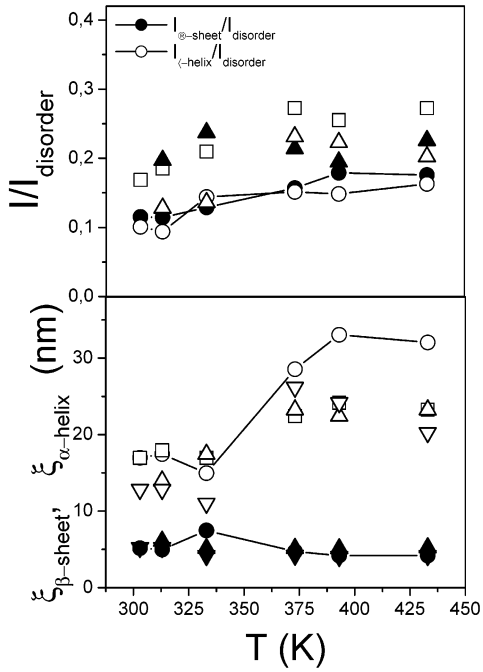

Figure 9. Top: Relative populations of the ordered peptide secondary structures, normalized according to the peptide volume fraction in the triblocks, as a function of temperature: (circles) $PBLG_{18}$, (squares) $PBLG_{22}-PEG_{21}-PBLG_{22}$, (up triangles) $PBLG_{17}-PEG_{90}-PBLG_{17}$, and (down triangles) $PBLG_{16}-PEG_{138}-PBLG_{16}$. Open and filled symbols reflect the ordered α-helical and β-sheet structures, respectively. Bottom: Temperature dependence of the associated correlation lengths. Notice the lower lengths for the β-sheet secondary structures as compared to the more coherent α-helical structures.

α-helical conformations whereas the band at ~1630 cm^{-1} is the shifted amide I band (amide C=O stretch) component to lower frequencies characteristic of the β-sheet conformation.[24,25] The latter has been assigned to increased H-bond strength; however, experiments on ^{13}C-labeled peptides and ab initio calculations have shown that the origin of the low-frequency β-sheet amide I band is due to multistranded clusters of extended β-strands.[25] Nevertheless, the FTIR results provide unambiguous evidence for the existence of the two secondary structures in agreement with the WAXS results.

Figures 6 and 7 show temperature-dependent WAXS and FTIR spectra of the $PBLG_{22}-PEG_{21}-PBLG_{22}$ (f_{rod} = 0.65) triblock copolymer obtained on cooling from 433 to 303 K, i.e., under identical thermal conditions. The WAXS spectra reveal the presence of the α-helical secondary structure in the usual hexagonal lattice. Furthermore, in agreement with the DSC results, there is no evidence for the sharp Bragg reflections associated with the monoclinic unit cell of PEG (with a unit cell parameter of 1.93 nm along the helix axis). The significant difference, however, from the pure peptide structure is the complete absence of the β-sheet structures from the copolymer diffraction patterns at all temperatures. The absence of the β-sheet structures from the copolymer can also be seen in FTIR with the absence of the band at 1630 cm^{-1} from the FTIR spectra shown at Figure 7. The short PEG block in the copolymer destabilizes the β-sheet conformations of the peptide chains. As we will discuss below, interfacial mixing plays an important role on the stability of the secondary structures. Nevertheless, the predominance of the α-helical secondary structures implies that the PBLG−PEG−PBLG copolymers have a rod−coil−rod structure.

The effect of increasing the volume fraction on the organization of the PBLG blocks can be better discussed by studying separately the effect of increasing the PEG degree of polymerization keeping the PBLG fixed or by increasing the PBLG degree of polymerization keeping the PEG fixed (Figure 8). The effect of increasing the PEG content while keeping the peptide units approximately constant is shown in the top of the figure by comparing the homopolymer and triblock copolymer diffraction patterns at 433 K. As discussed earlier, in $PBLG_{22}-PEG_{21}-PBLG_{22}$ (f_{rod} = 0.65), the β-sheet structures are completely absent but start to reappear in the copolymers with the lower peptide fraction (in $PBLG_{17}-PEG_{90}-PBLG_{17}$, f_{rod} = 0.25, and in $PBLG_{16}-PEG_{138}-PBLG_{16}$, f_{rod} = 0.17). A more subtle effect is the comparison of triblocks with a constant PEG degree of polymerization but with a variable PBLG content shown in the bottom of Figure 8. Apparently, increasing the peptide volume fraction has the same effect as above, however, this comparison is not straightforward since the peptide secondary structures are functions of the peptide length as well.

To make a more quantitative comparison of the relative populations of the peptide secondary conformations in PBLG and in the triblock copolymers we have modeled the broad diffractions peaks as a summation of Lorentzians

$$S(q) = S_{\beta}(q) + S_{\alpha}(q) + S_{amorp}(q) \qquad (1)$$

corresponding to the β-sheet, α-helical, and "amorphous halo" contributions with

$$S_i(q) = \frac{S(q^*)}{1 + \xi^2(q - q^*)^2} \qquad (2)$$

centered around the respective q^* with a corresponding correlation length ξ. This type of analysis models the diffractions patterns by the additive contribution from β-sheet structures (centered at $q^* \sim 3.5$ nm^{-1}), from α-helical structures (centered around 4.7 nm^{-1}) and a broad amorphous halo comprising mainly from the disordered side chains (centered around 14 nm^{-1}). The relative intensity ratio of the β-sheet and α-helical secondary peptide conformations in PBLG and in the triblocks is depicted in Figure 9. Of the $PBLG_{18}$ chains adopting an ordered secondary structure about half are organized in the ordered α-helical conformation. Notice also that there is a temperature dependence with a tendency to decrease the fraction of ordered chains in a secondary conformation with decreasing temperature as the glass transition of the peptide is approached. Similar trends are obtained in the copolymers.

A structural property that distinguishes the nanoscale structures that are related to the different peptide secondary structures is their coherence. The correlation lengths of α-helices are higher (more coherent structures) than the corresponding β-sheet secondary structures as shown in Figure 9. For example, correlation lengths in the range from 30 to 15 nm (by decreasing temperature) are found for the α-helical structures whereas only a range from 10 to 5 nm is found for the β-sheet conformations. Clearly, the latter structures are less coherent and this property could be related with their absence in the triblock copolymers with the higher peptide content.

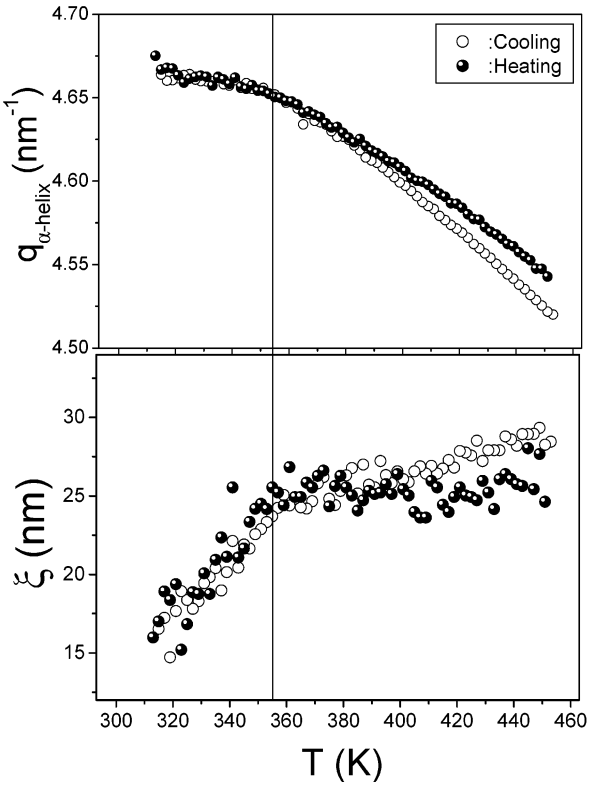

Figure 10. Temperature dependence of (top) the wavevector corresponding to the primary reflection of α-helices and (bottom) of the correlation length, obtained on cooling (open circles) and subsequent heating (filled circles) of $PBLG_{22}-PEG_{21}-PBLG_{22}$, with a rate of 2 K/min using synchrotron SAXS. Notice the different behavior below and above 355 K, associated with the 7/2 to 18/5 helix-to-helix transformation.

To further investigate the size, coherence and stability of the α-helical structures within the PBLG block in more detail, we performed synchrotron SAXS/WAXS experiments by following a slow heating/cooling circle as well as by performing temperature-jump experiments between 313 and 453 K. The result from the slow heating/cooling circle of $PBLG_{22}-PEG_{21}-PBLG_{22}$ (f_{rod} = 0.65) on the structural characteristics of the ordered α-helical secondary structure is shown in Figure 10. Notice the different temperature dependence of the characteristic wave vector at q^* below and above 357 K which, based on the DSC result, is associated with the reversible 7/2 to 18/5 helical conformation in the triblock. This $q^*(T)$ results in a dq^*/dT of 1.9×10^{-4} and 1.5×10^{-3} K^{-1} below and above the transition, respectively (following the cooling cycle), reflecting vastly different thermal expansion coefficients of the 7/2 and 18/5 helices. In addition, the correlation lengths associated with the thermodynamically more stable (18/5) helical conformation are substantially higher than of the corresponding 7/2 conformation at lower temperatures. The kinetics of the reversible 18/5 to 7/2 helical transformations studied between two temperatures i.e., 313 (7/2) and 453 K (18/5) were found to be very fast, both taking place within the first 60 s. The lack of an incubation period could be mistaken as suggesting spinodal decomposition for the transformation mechanism; however, the fast kinetics probably arise from a nucleation and growth mechanism applicable to first-order transitions as a result of the deep undercooling ($\Delta T \sim 40$ K). This point requires further investigation by performing kinetic experiments at lower quench depths.

The diffraction and FTIR studies, revealed that depending on the peptide volume fraction, there are substantial changes of the peptide secondary structures as well as on the ability of PEG to crystallize. To obtain a better understanding of these structural changes, we have investigated the degree of mixing of the two blocks by employing X-ray scattering on the pertinent length scale (i.e., SAXS). As an example, Figure 11 shows the SAXS pattern from the triblock $PBLG_{17}-PEG_{90}-PBLG_{17}$ with $f_{rod} = 0.25$. The pattern exhibits the usual peak of microphase separated block copolymers[26] with a corresponding distance of about 10 nm and higher order peaks. In the same Figure the SAXS pattern from the triblock copolymer $PBLG_{105}-PEG_{90}-PBLG_{105}$ with $f_{rod} = 0.67$ is also shown. The latter exhibits a broad liquidlike structure factor with the absence of higher

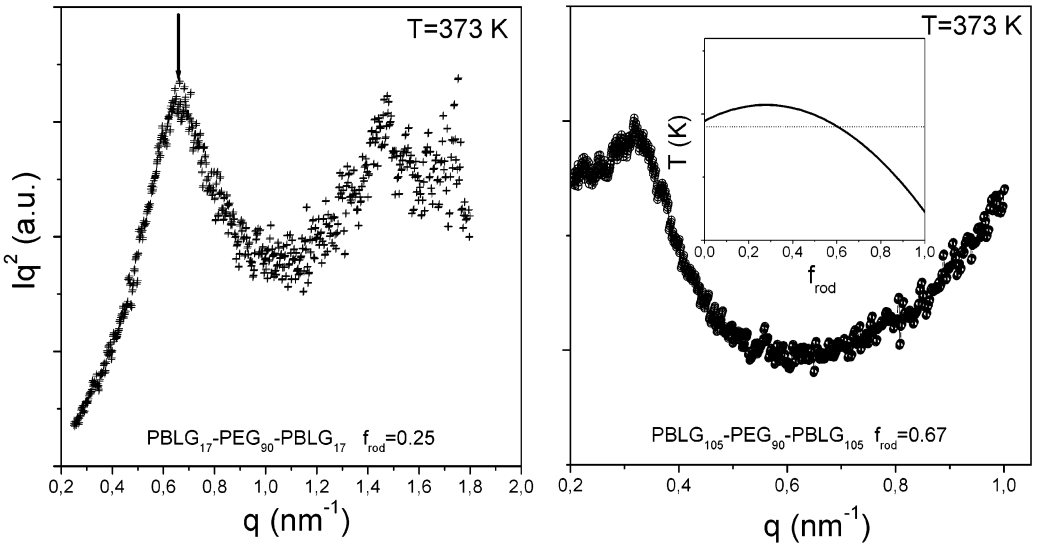

Figure 11. Left: SAXS profile of $PBLG_{17}-PEG_{90}-PBLG_{17}$ ($f_{rod} = 0.25$) at 373 K indicating the formation of a microphase separated structure with a characteristic spacing of 10 nm. Right: SAXS profile of $PBLG_{105}-PEG_{90}-PBLG_{105}$ ($f_{rod} = 0.67$) at 373 K indicating only weak phase separation (broad main peak and absence of higher order reflections). In the inset a highly schematic "phase diagram" is shown indicating stronger microphase separation for the triblocks with the lower peptide content, in accord with the SAXS study.

Table 2. Phase State of the PBLG−PEG−PBLG Triblock Copolymers[a]

compound name	f_{PBLG}	microphase separation (SAXS)	peptide secondary structure	PEO cryst (DSC)
$PBLG_9-PEG_{138}-PBLG_9$	0.1	+	α/β	+
$PBLG_8-PEG_{90}-PBLG_8$	0.135	+	α/β	+
$PBLG_{16}-PEG_{138}-PBLG_{16}$	0.17	+	α/β	+
$PBLG_{17}-PEG_{90}-PBLG_{17}$	0.25	+	α/β	+
$PBLG_9-PEG_{21}-PBLG_9$	0.43	−	α	−
$PBLG_{58}-PEG_{90}-PBLG_{58}$	0.53	−	α	−
$PBLG_{22}-PEG_{21}-PBLG_{22}$	0.65	−	α	−
$PBLG_{105}-PEG_{90}-PBLG_{105}$	0.67	−	α	−
$PBLG_{54}-PEG_{21}-PBLG_{54}$	0.82	−	α	−
$PBLG_{96}-PEG_{21}-PBLG_{96}$	0.89	−	α	−

[a] Key: (+) presence of microphase separation, PEO crystallization; (−) absence of microphase separation, PEO crystallization.

order reflections suggesting phase mixing.

The results on the phase state and its consequences on PEG crystallization and PBLG secondary structures are summarized in Table 2. Depending on the rod volume fraction, two cases can be distinguished: for low peptide volume fractions, the main and higher order SAXS peaks are intense, meaning that the triblock copolymers are more microphase separated. When $f_{rod} > 0.4$, only weak microphase separation exists based on the SAXS patterns. This is depicted as an inset to Figure 11 where a "phase diagram" is schematically shown by plotting the temperature corresponding to microphase separation as a function of the peptide volume fraction. The horizontal line, shows the phase state across the different volume fractions at a particular temperature and suggests phase mixing at higher peptide content. Interfacial mixing in the case of the higher peptide volume fractions has profound consequences on the peptide and PEG secondary structures: the less coherent peptide structures (β-sheet) are destabilized by the presence of the PEG chains which in turn cannot chain fold to crystallize. We mention that the absence of the β-sheet structures in the block copolymers with low peptide degrees of polymerization ($PBLG_9-PEG_{21}-PBLG_9$ and $PBLG_{22}-PEG_{21}-PBLG_{22}$) is purely due to mixing since pure peptides with the same low PBLG degrees of polymerization would form both α-helices and β-sheets. It is likely that the β-sheet secondary structures are located near the interface and thus become more unstable on mixing. On the other hand, the more coherent α-helical secondary structures persist on mixing. The fact that the latter structures (with a heat of fusion of 10 J/g) are more stable than the chain-folded PEG (with a heat of fusion of 40−50 J/g) may reflect the higher strength of the hydrogen bond in comparison to the van der Waals forces.

These structural characteristics in the triblock copolymers can be captured by the schematic model shown in Figure 12. The figure on the top depicts the experimental case under low peptide volume fractions: columnar hexagonal arrangement of α-helical peptides with correlation lengths of about 20 nm, with an intercylinder distance of 1.2 nm and a cylinder length of about 3 nm (for the $PBLG_{18}$), separated from semicrystalline PEG chains within a length scale of 10 nm. The figure on the bottom depicts the experimental case corresponding to the copolymers with the higher peptide volume fractions: only the α-helical peptides in the columnar hexagonal arrangement can survive the interfacial mixing. Thus, mixing provides the means to control the appearance of certain peptide secondary structures. Last, we mention that the second case of

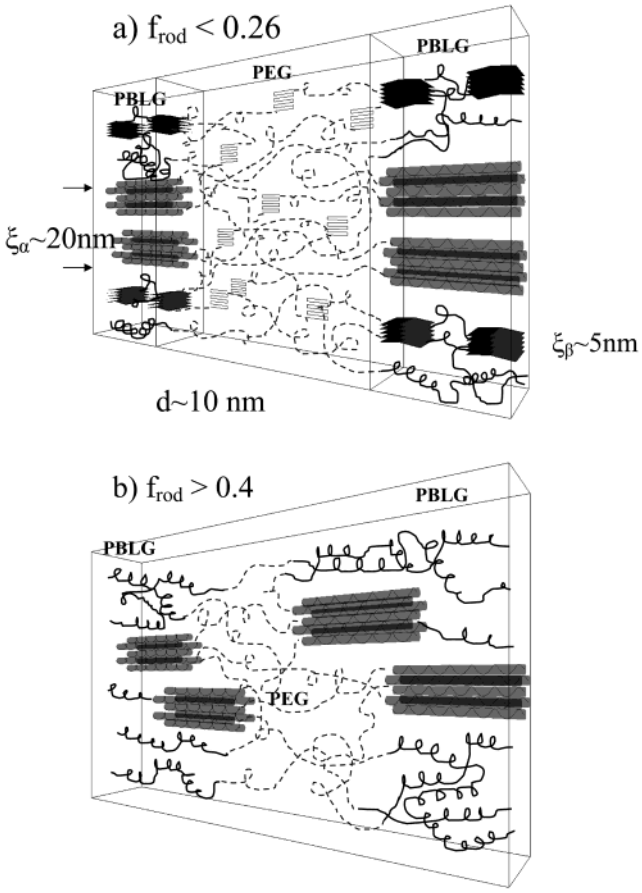

Figure 12. Highly schematic model of the phase state in the PBLG−PEG−PBLG triblock copolymers. Top: phase state corresponding to low peptide volume fractions depicting a microphase separated copolymer consisting of all the peptide and PEG secondary structures. Bottom: phase state corresponding to $f_{rod} > 0.4$ depicting phase mixing resulting in the appearance of only one (α-helical) secondary structure.

Figure 12 would not be possible with a diblock copolymer of the same length since the critical value of the product χN, where χ is the interaction parameter and N is the total degree of polymerization, is lower for a diblock copolymer meaning that a diblock copolymer would be phase separated at the studied temperatures.

4. Conclusions

The tandem molecular interactions in PBLG−PEG−PBLG rod−coil−rod triblock copolymers give rise to unanticipated structural changes for both blocks.

1. Low molecular weight PBLG is a mixture of lamellar assembly of β-sheet, columnar hexagonal ar-

rangement of α-helical peptides, and disordered helices. Increasing temperature results in an increase of both β-sheet and α-helical conformations and their ratio remains practically unchanged.

2. The tandem molecular interactions present in the copolymers give rise to three levels of organization: first, the hydrogen bonds present in the peptide blocks stabilize the peptide secondary structures (α-helices and β-sheets), and in addition, chain folding occurs in PEG; second, the α-helical and β-sheet secondary structures are packed in hexagonal and orthogonal unit cells, respectively; and third, the repulsive interactions between the unlike blocks give rise to nanostructures typical of phase separated block copolymers.

3. On the basis of the peptide volume fraction, two cases were found: for low peptide fractions, microphase separation results in PBLG and PEG phases rich in all secondary structures (α-helix, β-sheet, and chain-folded PEG). However, for the PEG midblock, large undercooling ($\Delta T \approx 50$ K) is necessary as a result of the confinement. Increasing the peptide volume fraction results in interfacial mixing of the two blocks. Under such conditions only the more coherent peptide secondary structure (α-helices) can survive.

4. The irreversible 7/2 to 18/5 helical conformation in the peptides becomes reversible in the copolymers.

These structural characteristics in the copolymers were not anticipated, however, there are still some issues that remain unresolved. For example, the reason that the irreversible 7/2 to 18/5 helix-to-helix transformation in the pure peptides becomes reversible in the copolymers is not clear at present. In addition, a complete phase diagram is still lacking mainly because of the low SAXS contrast for microphase separation. In that sense, it would be of interest to investigate peptide-based copolymer systems with stronger interactions. A step forward in this direction is the synthesis of block copolymers based on poly(dimethylsiloxane)− (PDMS−) PBLG.

Acknowledgment. This work was supported in part by a GSRT grant (PENED2001) to G.F. and P.P., the Fonds der Chemischen Industrie, the Bundesministerium für Bildung und Forschung, the Deutsche Forschungsgemeinschaft (Emmy Noether Program, H.-A.K.) and the International Max Planck Research School. S. Prehl is gratefully acknowledged for her help with the synthetic part of the work and D. W. Scholdei for his assistance with the FTIR experiments.

References and Notes

(1) Muthukumar, M.; Ober, C. K.; Thomas, E. L. *Science* **1997**, *277*, 1225−1232.
(2) Stupp, S. I.; Braun, P. V. *Science* **1997**, *277*, 1242−1248.
(3) Kovacs, A. J.; Ginthier, A. *Kolloid Z. Z. Polym.* **1972**, *250*, 530.
(4) Block, H. In *Poly(γ-benzyl-L-glutamate) and other glutamic acid containing polymers*; Gordon and Breach Science Publishers: New York, 1983.
(5) Yu, S. M.; Conticello, V. P.; Zhang, G.; Kayser, Ch.; Fournier, M. J.; Mason, T. L.; Tirrell, D. A. *Nature (London)* **1997**, *389*, 167−170.
(6) Yu, S. M.; Soto, C. M.; Tirrell, D. A. *J. Am. Chem. Soc.* **2000**, *122*, 6552−6559.
(7) He, S.-J.; Lee, C.; Gido, S. P.; Yu, S. M.; Tirrell, D. A. *Macromolecules* **1998**, *31*, 9387−9389.
(8) Harrison, P. M.; Bamborough, P.; Duggett, V.; Prusiner, S. B.; Cohen, F. E. *Curr. Opin. Struct. Biol.* **1997**, *7*, 53−59.
(9) Nishimura, T.; Sato, Y.; Yokoyama, M.; Okuya, M.; Inoue, S.; Kataoka, K.; Okano, T.; Sakurai, Y. *Makromol. Chem.* **1984**, *185*, 2109−2116.
(10) Kugo, K.; Ohji, A.; Uno, T.; Nishino, J. *Polym. J.* **1987**, *19*, 375−381.
(11) Cho, C. S.; Kim, S. W.; Komoto, T. *Makromol. Chem.* **1990**, *191*, 981−991.
(12) Poche, D. S.; Moore, M. J.; Bowles, J. L. *Synth. Commun.* **1999**, *29*, 843−854.
(13) Klok, H.-A.; Langenwalter, J. F.; Lecommandoux, S. *Macromolecules* **2000**, *33*, 7819−7826.
(14) Lecommandoux, S.; Achard, M.-F.; Langenwalter, J. F.; Klok, H.-A. *Macromolecules* **2001**, *34*, 9100−9111.
(15) Zalipsky, S.; Gilon, C.; Zilkha, A. *Eur. Polym. J.* **1983**, *19*, 1177−1183.
(16) Floudas, G.; Tsitsilianis, C. *Macromolecules* **1997**, *30*, 4381−4390.
(17) Watanabe, J.; Uematsu, I. *Polymer* **1984**, *25*, 1711−1717.
(18) Loo, Y.-L.; Register, R. A.; Ryan, A. J.; Dee, G. T. *Macromolecules* **2001**, *34*, 8968−8977.
(19) Loo, Y.-L.; Register, R. A.; Ryan, A. J. *Macromolecules* **2002**, *35*, 2365−2374.
(20) Schipper, F. J. M.; Floudas, G.; Pispas, S.; Hadjichristidis, N.; Pakula, T. *Macromolecules* **2002**, *35*, 8860−8868.
(21) Papadopoulos, P.; Floudas, G.; Klok, H.-A. To be published.
(22) Komoto, T.; Kim, K. Y.; Kawai, T. *Makromol. Chem.* **1978**, *179*, 373−385.
(23) Elliott, A.; Fraser, R. D. B.; MacRae, T. D. *J. Mol. Biol.* **1965**, *11*, 821.
(24) Miyazawa, T.; Blout, E. R. *J. Am. Chem. Soc.* **1961**, *83*, 712−719.
(25) Kubelka, J.; Keiderling, T. A. *J. Am. Chem. Soc.* **2001**, *123*, 6142−6150.
(26) See, for example: *Block Copolymers. Synthetic strategies, physical properties and applications*; Hadjichristidis, N., Pispas, S., Floudas, G., Eds.; J. Wiley: New York, 2002.

MA025918K